Anomalous doping evolution of nodal dispersion revealed by *in situ* ARPES on continuously doped cuprates

Yigui Zhong,[1,2] Jianyu Guan,[1,2] Jin Zhao,[1,2] Cenyao Tang,[1,2] Zhicheng Rao,[1,2] Haijiang Liu,[1,2] Jianhao Zhang,[3] Sen Li,[3] Zhengyu Weng,[3] Genda Gu,[4] Yujie Sun,[1,5,*] and Hong Ding[1,2,5,†]

[1]*Beijing National Laboratory of Condensed Matter Physics and Institute of Physics, Chinese Academy of Sciences, Beijing 100190, China*

[2]*School of Physics, University of Chinese Academy of Sciences, Beijing 100049, China*

[3]*Institute for Advanced Study, Tsinghua University, Beijing 100084, China*

[4]*Condensed Matter Physics and Materials Science Department, Brookhaven National Laboratory, Upton, New York 11973, USA*

[5]*Songshan Lake Materials Laboratory, Dongguan, Guangdong 523808, China*

(Received 27 June 2019; revised manuscript received 16 October 2019; published 5 November 2019)

We study the systematic doping evolution of nodal dispersions by *in situ* angle-resolved photoemission spectroscopy on the continuously doped surface of a high-temperature superconductor $Bi_2Sr_2CaCu_2O_{8+x}$ and reveal that the nodal dispersion has three fundamentally different segments separated by two kinks, located at ∼10 meV and roughly 70 meV, respectively. These three segments have different band velocities and different doping dependence. In particular, in the underdoped region the velocity of the high-energy segment increases monotonically as the doping level decreases and can even surpass the bare band velocity. We propose that electron fractionalization is a possible cause for this anomalous nodal dispersion and may even play a key role in the understanding of exotic properties of cuprates.

DOI: 10.1103/PhysRevB.100.184504

I. INTRODUCTION

For the high-temperature (high-T_c) cuprates, one of the puzzling features is the "kink" in the electronic band dispersion, which universally exists in different superconducting families of cuprates [1–3]. Along the nodal direction of the d-wave superconducting gap, the kink appears at a binding energy of roughly 70 meV in many cuprates [1,4–6]. Meanwhile near the antinode with the maximum energy gap, a seemingly stronger kink is located at about 20–40 meV [7–9], depending on the doped carrier concentration x. Many scenarios have been proposed to understand the origin of this kink feature [10–12]. For examples, one popular proposal is that a strong electron-phonon coupling induces a kink in the dispersion [13,14], while another one suggests that the electron-magnetic mode coupling is responsible for the kink [15–17]. Yet the origin of this universal kink is far from settled. Recently we developed a technique to continuously change the doping level of surface layers by annealing a sample in ozone/vacuum atmosphere, which enables a systematic *in situ* angle-resolved photoemission spectroscopy (ARPES) study on the same surface with a wide range of doping level, thus promising more precise studies on doping evolution of many important properties of the cuprates [18].

In this paper, we systematically study the doping evolution of the nodal dispersion by performing *in situ* ARPES measurements on a continuously doped surface of $Bi_2Sr_2CaCu_2O_{8+x}$ (Bi2212). From the measured band dispersions, two kinks are identified at ∼10 and 45–70 meV below the Fermi level (E_F), respectively, and they separate the nodal dispersion into three segments with different band velocities. We clearly demonstrate the fundamentally different doping evolutions for these three band velocities: a decreasing velocity for the lower segment, a no-change velocity for the middle segment, and an increasing velocity for the higher segment, as the doping level decreases. What is more exotic is that the velocity of the higher segment becomes divergent and can even exceed the bare band velocity for the extremely underdoped (UD) ones. After discussing several possible scenarios proposed to explain the kink phenomena, we suggest that electron fractionalization at high energy is likely responsible for the anomalous doping evolution of the nodal dispersion in the UD region.

II. METHODS

Sample preparation and surface treatment of ozone/vacuum annealing to continuously change the doping level of surface layers were described in our previous paper [18]. *In situ* ARPES measurements were performed in a laboratory ARPES system equipped with a Scienta R4000 analyzer and a Scienta VUV light source. He-Iα resonant line ($h\nu$ = 21.218 eV) was used and the vacuum of the ARPES chamber was better than 3×10^{-11} Torr. The energy and angle resolution were set as ∼5 meV and ∼0.2°, respectively. All data in this paper were acquired at 12 K to make sure the sample surface at all doping levels is in the superconducting state.

III. RESULTS AND DISCUSSION

We first show the spectrum image plots with the same color scale along the nodal direction at various different

*Corresponding author: yjsun@aphy.iphy.ac.cn
†Corresponding author: dingh@iphy.ac.cn

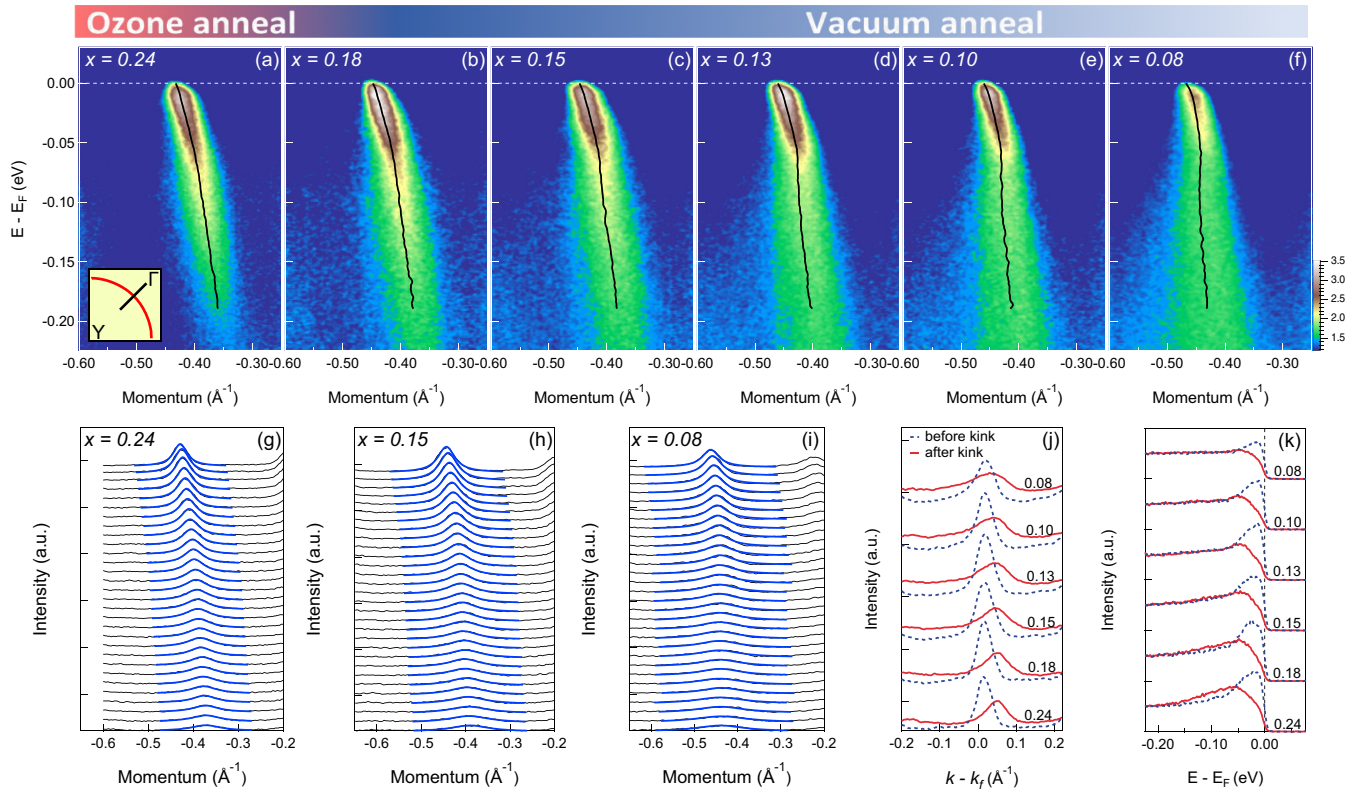

FIG. 1. (a) ARPES spectrum of ozone-annealed Bi2212 along the nodal direction (as illustrated in the inset), the doping level is estimated as 0.24. Ozone anneal means sample is annealed at ozone atmosphere. (b)–(f) Spectra acquired from the same sample surface after annealed in vacuum with different temperatures (called vacuum anneal) step by step, and the corresponding doping levels are estimated as 0.18, 0.15, 0.13, 0.10, and 0.08, respectively. These spectra are plotted in the same color scale as illustrated in the lower right side of (f). (g)–(i) The black lines are the raw MDC plots for the doping levels at 0.24, 0.15, and 0.08, respectively, and the blue lines are their Lorentzian fittings. (j) The MDCs before the kink (blue dashed lines, $E - E_F = -27$ meV) and after the kink (red solid lines, $E - E_F = -105$ meV) at different doping levels. (k) The EDCs before the kink (blue dashed lines, $k - k_f = 0.017$ Å^{-1}) and after kink (red solid line, $k - k_f = 0.043$ Å^{-1}) at different doping levels.

doping levels from $x \sim 0.24-0.08$ [Figs. 1(a)–1(f)], which were acquired on the same surface through annealing the sample in the ozone/vacuum circumstance [19]. The well-known 70-meV kink is clearly observed at each doping level, and the spectral intensity has a sudden reduction after crossing the kink. The area with high intensity (light color in images) shrinks dramatically when it goes to the UD region. Interestingly, the band beyond the kink becomes more and more vertical, which indicates that the kink becomes stronger with decreasing doping level. In order to extract the band dispersion for quantitative comparison, a standard practice [20] is to perform a Lorentzian fitting to momentum distribution curves (MDCs) that are intensity distributions as a function of momentum at a fixed energy [Figs. 1(g)–1(i)], with an assumption that the self-energy (SE) in the Green's function has no or weak dependence on momentum. From the fitting, the peak positions of MDCs trace out the band dispersion and the widths contain the information of the quasiparticle lifetime. The extracted band dispersion for each doping level is plotted with the black lines in Figs. 1(a)–1(f). Again, one can clearly see that the kink phenomena become stronger with decreasing doping level. The spectral width is also seen to become wider as the doping level decreases [Figs. 1(g)–1(i)]. Meanwhile, the spectral width becomes larger suddenly when it passes across the kink [Figs. 1(j) and 1(k)], indicating an abrupt change of the quasiparticle lifetime.

In principle, ARPES probes the single-particle spectral function, which treats the many-body interactions as additional SE renormalization to electrons [21]. One way to understand the interactions in a material is to analyze the SE $\Sigma(w)$ from ARPES spectra. By comparing the measured band with its corresponding bare band [Fig. 2(a)], one can extract the real part ReΣ, which is the energy difference between the measured band and the bare band, and the imaginary part ImΣ, which is proportional to the MDC width. According to previous practices [22], the low-energy bare band along the nodal direction in the cuprates can be approximated as a linear line that connects the measured Fermi crossing point and the higher binding energy, typically around ~200 meV. We note that there are other different forms for the bare band used in previous literature [23]. For direct comparison, the MDC-derived nodal dispersions at different doping levels are plotted with the relative momentum to their corresponding Fermi momenta (k_F) [Figs. 2(a) and 3(a)]. We notice that previous literature [1,4–9] usually plot the real part ReΣ and the MDCs' width in the binding energy [Figs. 2(b) and 2(d)] due to the weak dependence on momentum. In order

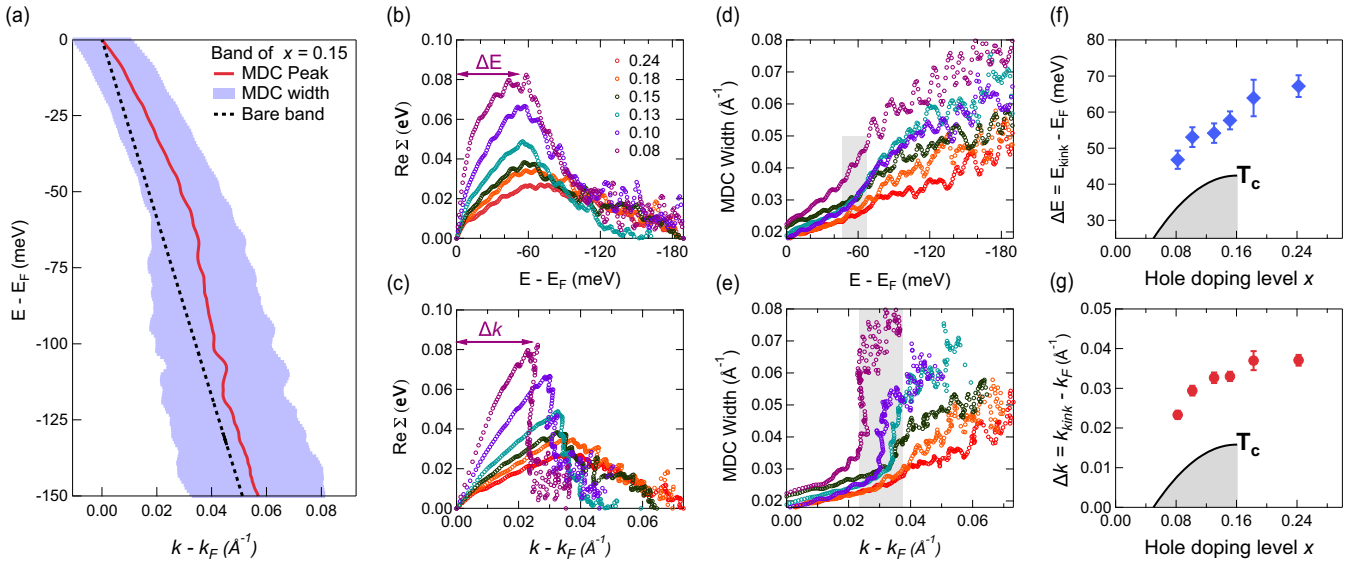

FIG. 2. (a) MDC-derived band dispersion at the doping level equals 0.15: the red line is the peak of MDCs extracted by Lorentzian fitting, and the violet shadow represents the width of MDCs. The dashed line is a typical bare band as described in the text. (b),(c) The real parts of SE at each doping level are plotted against with the binding energy in (b) and with the peak's position of the corresponding MDCs in (c). The double-headed arrows indicate how we extract the energy positions $\Delta E(x)$ and momentum position $\Delta k(x)$ respectively. (d),(e) Same as (b) and (c) but for the MDCs width at each doping level. The shadow regions in (d) and (e) highlight the dramatic changes of the MDCs width. (f),(g) The determined $\Delta k(x)$ and $\Delta E(x)$ for each doping level. The black lines along with the shadow domes represent the UD side of the superconducting dome.

to better visualize the SE, we also plotted ReΣ and MDCs' width against the peak positions of the fitted MDCs [Figs. 2(c) and 2(e)]. One can see the conspicuous peaks in ReΣ curves [Figs. 2(b) and 2(c)], which indicates that there is a large renormalization of the electronic dispersion at where the kink occurs. The energy position of the kink [Fig. 2(f)] and relative momentum position of the kink [Fig. 2(g)] for different doping levels can be identified through these conspicuous peaks. With decreasing doping level, the peak in ReΣ curves gradually grows and moves to the E_F or k_F and its height is enhanced due to the stronger kink. Meanwhile the width of MDCs dramatically increases after the kink for the UD samples, while it is much milder before the kink [Figs. 2(d) and 2(e)]. This behavior becomes more and more noteworthy as the doping level decreases, especially in the UD side. It resembles electrons undergoing a decay from a well-defined quasiparticle to something with an extremely short lifetime when they go across the kink. What is more impressive is that the kink gradually moves toward their corresponding k_F and E_F with decreasing doping level in the UD side, which directly suggests the area with a well-defined quasiparticle shrinks [Figs. 2(f) and 2(g)].

Since the quasiparticle lifetime experiences a large transformation after crossing the kink, we next study the effective mass of the band dispersion before and after the kink. The MDC-derived nodal band dispersions at different doping levels are summarized in Figs. 3(a)–3(c). Besides the kink at 45–70 meV, one can see another kink of the band dispersion at a lower binding energy ~10 meV [19], which contributes a "shoulder" in the ReΣ curves [Fig. 2(b)] and becomes more pronounced at the UD levels [Fig. 3(a)]. These two kinks separate the nodal band dispersion into three segments with different band velocities or effective masses. To make the results more precise, we avoid the vicinity of these two kinks and evaluate velocities of three band segments at the binding energy of 0–5 meV(v_l), 25–55 meV(v_m), and 80–125 meV(v_h) [Fig. 3(d)]. We note that the energy range to evaluate the middle-range velocity varies slightly for different doping levels in order to avoid the nearby low-energy kink. The numerical analysis of doping dependence on the velocities of three band segments is displayed in Fig. 3(e). We find that the v_l just below E_F decreases smoothly with decreasing doping level [Fig. 3(b)], which is consistent with the theoretical expectation that stronger electron-electron interactions at UD samples shall make electrons heavier [24]. The v_m remains a constant [Fig. 3(c)] over a wide doping range, consistent with previous observations [25,26]. The exotic behavior is that the v_h at the higher binding energy dramatically increases with decreasing doping level in the UD region, in opposite with the expected trend. More surprisingly, at the heavily UD level the v_h can even surpass its bare band velocity which is defined by LDA calculations [27,28]. Those exotic behaviors of the velocity imply an unconventional origin of the kink in the nodal dispersion.

The popular scenario of kink origin attributes these phenomena in electronic dispersion as the renormalized effect to the electrons due to the electrons coupling with some kinds of bosonic mode at specific energies, like phonons or spin resonance [1,13–17]. Although some of these bosonic modes do exist in the cuprates [29–31], these coupling scenarios are unable to explain the doping dependence of the kink phenomena, especially in the aspect of the divergent v_h. The magnetic resonance mode scenario is unlikely since the kink in the nodal dispersion still robustly survives in the normal

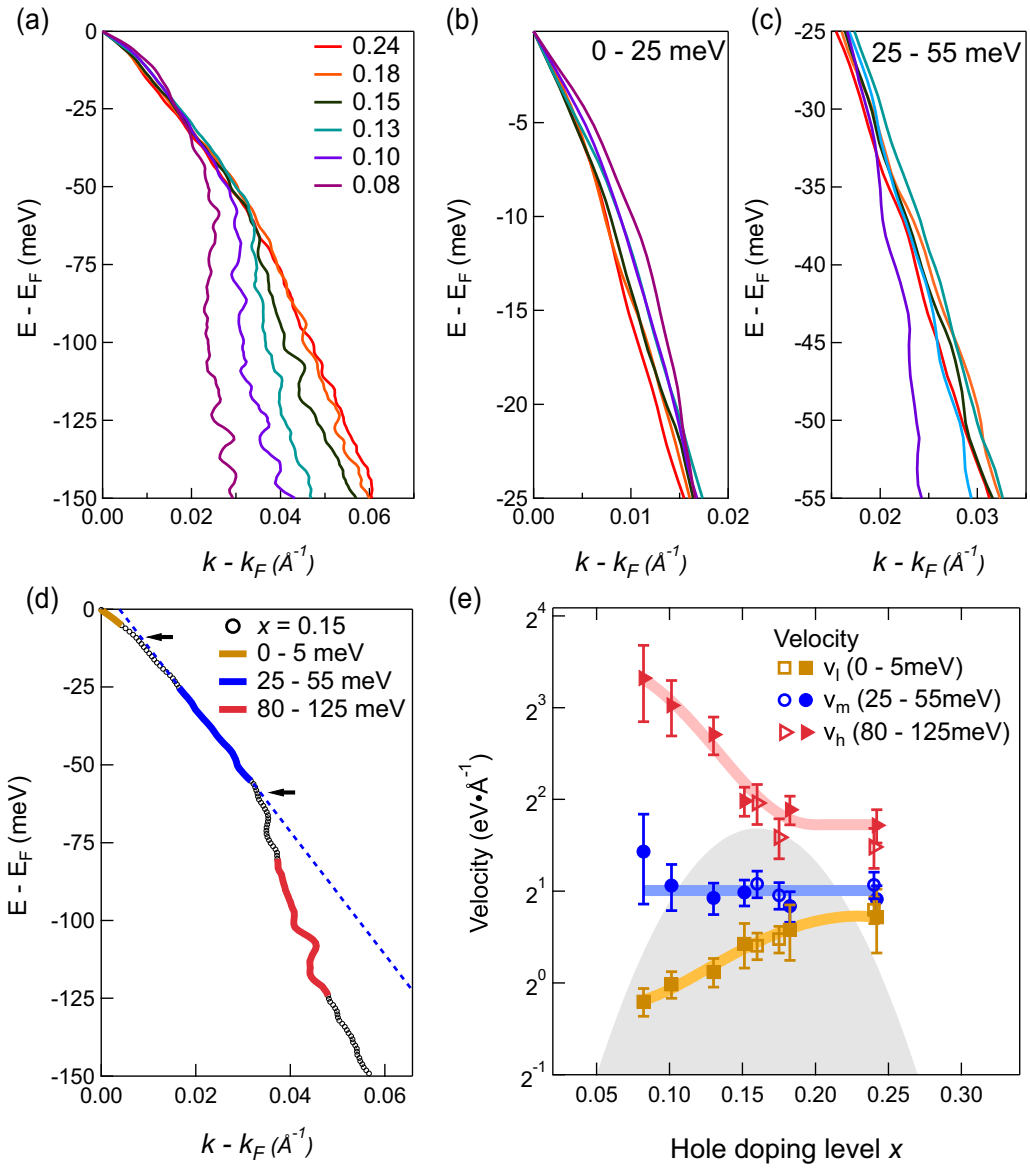

FIG. 3. (a) Summary of MDC-derived nodal dispersions at different doping levels. The momentum is scaled to their corresponding k_F. (b) The MDC-derived nodal dispersion segments at the binding energy range with 0–25 meV. (c) The MDC-derived nodal dispersion segments at 25–55 meV. (d) Three segments separated by two kinks which are marked with the black arrows: the brown one marks the segment at 0–5meV, the blue one marks the segment at 25–55 meV, the red one marks the segment at 80–125 meV. The black circles are the nodal dispersion at the doping level which equals 0.15. (e) The doping evolution of velocities of three segments plotted with the corresponding colors marked in (d). The empty markers with corresponding shapes represent an independent data set acquired from another sample. The colored shadow lines are guides for eyes. The gray shadow dome represents the superconducting phase region.

states where the magnetic resonance mode vanishes [1,31], so here we focus on discussing the electron-phonon coupling (EPC) scenario. First, under the frame of the EPC, typically the bare bands can be regarded approximately as a linear line within a narrow energy window that connects the measured E_F and a higher binding energy just like the dashed line in Fig. 2(a). Thus, with decreasing doping level, due to the increasing v_h, the bare bands will become more and more vertical, which is directly incompatible with the simple rigid-band shift picture of Bi2212 [32,33]. Second, according to the weak EPC scenario described by the Migdal-Eliashberg picture [34], since the EPC domain should be restricted to a small energy range around the typical energy of phonon modes (Ω), the dispersion well above Ω tends to be recovered to the position of the noninteracting band. Thus, the band velocity of the segment at a higher binding energy than Ω will remain relatively stable, and for the binding energy lower than Ω, the corresponding velocity will change with the coupling strength, which is opposite to what was observed here. Third, we noticed the strong EPC picture due to the formation of the polarons [35,36] is argued to be a proper explanation for the kinks in the undoped and lightly UD cuprates. However, a placid change of quasiparticle lifetime at the kink point and a more placid evolution of high-energy band velocity as a function of doping level inferred from polaronic scenario cannot capture our measurements here.

On the contrary, it is reasonable that the kink at the lower energy ∼10 meV stems from the EPC [26,37,38] due to that it fits well with the conventional coupling frame. The segments after the lower energy kink recovers to the noncoupling dispersion which has a constant velocity, while distinguishably the segments before the lower energy kink have different velocities due to variable strength of coupling. In fact, there is strong evidence of the existence of the lower energy phonons in Bi2212 [39].

We noticed that Randeria *et al.* [11] phenomenologically suggested that the $v_{\rm h}$ are a consequence of the renormalization to the nodal quasiparticle weight Z_k through a formula $v_h = v_m/Z_k$. Due to that the v_m is constant, the nodal quasiparticle weight Z_k should decrease quite rapidly with decreasing doping level, which is not consistent with our previous results that the nodal quasiparticle weight Z_k keeps relatively constant over a wide doping range [18].

The unconventional behavior of the $v_{\rm h}$ surpassing the predicted velocity of the bare band is reminiscent of the electron fractionalization in some of the one-dimensional (1D) materials [40,41]. Similar scenarios of electron fractionalization have also been proposed for the 2D cuprates [42–45]. For the parent compound of a cuprate superconductor, a Mott insulator, the charge is gapped due to strong on-site repulsive energy [46], while the spin has a gapless excitation [47], so the charge and spin degrees can be separated in the low-energy excited processes, namely, the electrons are fractionalized. With the holes doped into, the system gradually evolves into a high-T_c superconductor, and this fractionalization effect becomes weaker but still leaves some signatures in the UD region. In fact, there are many theoretical models suggesting that the spin-charge separation is the key to the cuprates [46,48–50]. One of these theoretical models is the so-called phase string theory [50]. In a doped Mott insulator described by the simplest t-J model [46], the doped holes cannot propagate coherently due to the presence of a nontrivial sign structure stemming from the phase string sign structure, which is distinct from the conventional fermion sign structure [50–52]. In order to incorporate the charge propagation properly, the doped holes should be fractionalized at a higher energy. The phase string theory [53] predicts that a peculiar electron fractionalization happens in the doping region accompanying the pseudogap, which intrinsically leads to a two-component structure: 1. The band segment before the 70-meV kink would be the "protected" emergent quasiparticle with the bare-band Fermi velocity, which is independent of the doped concentration x; 2. The segment after the kink acquires a larger band velocity due to the natural electronic fractionalization, which increases conspicuously with decreasing doping level, especially for very low doped ones. Naturally, due to the electron fractionalization, the spectra have a sudden broadening after crossing the kink. A comprehensive theoretical demonstration along this line is given in a separate paper [54], which nicely reproduced many features observed in our ARPES measurements.

IV. CONCLUSIONS

In conclusion, we conducted a systematic ARPES study of nodal dispersion of Bi2212 over a wide doping range and revealed that the velocity of the segment after the high-energy kink unconventionally increases with decreasing doping level in the UD region, which cannot be explained by the electron-mode coupling scenario. Alternatively, we propose the electronic fractionalization effect at high energy might be responsible for the unconventional behaviors.

ACKNOWLEDGMENTS

We thank J.-P Hu and Z.-Q. Wang for helpful discussion and F.-Z. Yang and J.-R. Huang for technical assistance. The work at the Institute of Physics was supported by the Ministry of Science & Technology of China (Grants No. 2016YFA0401000, No. 2015CB921300, and No. 2015CB921000), the Natural Science Foundation of China (Grants No. 11227903 and No. 11574371), the Chinese Academy of Sciences (Grants No. XDB07000000 and No. XDPB08-1), and Beijing Municipal Science & Technology Commission (Grant No. Z181100004218005). G.G. was supported by the Office of Basic Energy Sciences, Division of Materials Science and Engineering, U.S. Department of Energy, under Contract No. DE-SC0012704.

Y.Z. and J.G. contributed equally to this work.

[1] A. Lanzara, P. Bogdanov, X. Zhou, S. Kellar, D. Feng, E. Lu, T. Yoshida, H. Eisaki, A. Fujimori, and K. J. N. Kishio, Evidence for ubiquitous strong electron–phonon coupling in high-temperature superconductors, Nature (London) **412**, 510 (2001).

[2] T. Cuk, D. H. Lu, X. J. Zhou, Z. X. Shen, T. P. Devereaux, and N. Nagaosa, A review of electron–phonon coupling seen in the high-Tc superconductors by angle-resolved photoemission studies (ARPES), Phys. Status Solidi B **242**, 11 (2005).

[3] J. P. Carbotte, T. Timusk, and J. Hwang, Bosons in high-temperature superconductors: an experimental survey, Rep. Prog. Phys. **74**, 066501 (2011).

[4] P. V. Bogdanov, A. Lanzara, S. A. Kellar, X. J. Zhou, E. D. Lu, W. J. Zheng, G. Gu, J. I. Shimoyama, K. Kishio, and H. Ikeda, Evidence for an Energy Scale for Quasiparticle Dispersion in $Bi_2Sr_2CaCu_2O_8$, Phys. Rev. Lett. **85**, 2581 (2000).

[5] A. Kaminski, M. Randeria, J. C. Campuzano, M. R. Norman, H. Fretwell, J. Mesot, T. Sato, T. Takahashi, and K. Kadowaki, Renormalization of Spectral Line Shape and Dispersion Below Tc in $Bi_2Sr_2CaCu_2O_{8+\delta}$, Phys. Rev. Lett. **86**, 1070 (2001).

[6] P. D. Johnson, T. Valla, A. V. Fedorov, Z. Yusof, B. O. Wells, Q. Li, A. R. Moodenbaugh, G. D. Gu, N. Koshizuka, and C. Kendziora, Doping and Temperature Dependence of the Mass Enhancement Observed in the Cuprate $Bi_2Sr_2CaCu_2O_{8+\delta}$, Phys. Rev. Lett. **87**, 177007 (2001).

[7] J. C. Campuzano, H. Ding, M. R. Norman, H. M. Fretwell, M. Randeria, A. Kaminski, J. Mesot, T. Takeuchi, T. Sato, and T. Yokoya, Electronic Spectra and Their Relation to the (π, π)

Collective Mode in High-Tc Superconductors, Phys. Rev. Lett. **83**, 3709 (1999).

[8] T. Cuk, F. Baumberger, D. H. Lu, N. Ingle, X. J. Zhou, H. Eisaki, N. Kaneko, Z. Hussain, T. P. Devereaux, and N. Nagaosa, Coupling of the B_{1g} Phonon to the Antinodal Electronic States of $Bi_2Sr_2Ca_{0.92}Y_{0.08}Cu_2O_{8+\delta}$, Phys. Rev. Lett. **93**, 117003 (2004).

[9] A. D. Gromko, A. V. Fedorov, Y. D. Chuang, J. D. Koralek, Y. Aiura, Y. Yamaguchi, K. Oka, Y. Ando, and D. S. Dessau, Mass-renormalized Electronic Excitations at $(\pi, 0)$ in the Superconducting State of $Bi_2Sr_2CaCu_2O_{8+\delta}$, Phys. Rev. B **68**, 174520 (2003).

[10] E. Schachinger, J. J. Tu, and J. P. Carbotte, Angle-resolved photoemission spectroscopy and optical renormalizations: Phonons or spin fluctuations, Phys. Rev. B **67**, 214508 (2003).

[11] M. Randeria, A. Paramekanti, and N. Trivedi, Nodal quasiparticle dispersion in strongly correlated d-wave superconductors, Phys. Rev. B **69**, 144509 (2004).

[12] K. Matsuyama, E. Perepelitsky, and B. S. Shastry, Origin of kinks in the energy dispersion of strongly correlated matter, Phys. Rev. B **95**, 165435 (2017).

[13] T. P. Devereaux, T. Cuk, Z. X. Shen, and N. Nagaosa, Anisotropic Electron-Phonon Interaction in the Cuprates, Phys. Rev. Lett. **93**, 117004 (2004).

[14] H. S. Ruiz and A. Badía-Majós, Nature of the nodal kink in angle-resolved photoemission spectra of cuprate superconductors, Phys. Rev. B **79**, 054528 (2009).

[15] M. Eschrig and M. R. Norman, Neutron Resonance: Modeling Photoemission and Tunneling Data in the Superconducting State of $Bi_2Sr_2CaCu_2O_{8+\delta}$, Phys. Rev. Lett. **85**, 3261 (2000).

[16] D. Manske, I. Eremin, and K. H. Bennemann, Analysis of the Elementary Excitations in high-T_c Cuprates: Explanation of the New Energy Scale Observed by Angle-Resolved Photoemission Spectroscopy, Phys. Rev. Lett. **87**, 177005 (2001).

[17] D. S. Inosov, S. V. Borisenko, I. Eremin, A. A. Kordyuk, V. B. Zabolotnyy, J. Geck, A. Koitzsch, J. Fink, M. Knupfer, and B. Büchner, Relation between the one-particle spectral function and dynamic spin susceptibility of superconducting $Bi_2Sr_2CaCu_2O_{8-\delta}$, Phys. Rev. B **75**, 172505 (2007).

[18] Y. G. Zhong, J. Y. Guan, X. Shi, J. Zhao, Z. C. Rao, C. Y. Tang, H. J. Liu, Z. Y. Weng, Z. Q. Wang, and G. D. Gu, Continuous doping of a cuprate surface: Insights from *in situ* angle-resolved photoemission, Phys. Rev. B **98**, 140507 (2018).

[19] See Supplemental Material at http://link.aps.org/supplemental/10.1103/PhysRevB.100.184504 for the details of the evolution of the Fermi surface, nodal kF shift, superconducting gap, and the extraction of the nodal band dispersions and two kinks.

[20] T. Valla, A. V. Fedorov, P. D. Johnson, B. O. Wells, S. L. Hulbert, Q. Li, G. D. Gu, and N. Koshizuka, Evidence for quantum critical behavior in the optimally doped cuprate $Bi_2Sr_2CaCu_2O_{8+\delta}$, Science **285**, 2110 (1999).

[21] A. Damascelli, Z. Hussain, and Z.-X. Shen, Angle-resolved photoemission studies of the cuprate superconductors, Rev. Mod. Phys. **75**, 473 (2003).

[22] T. Valla, A. V. Fedorov, P. D. Johnson, and S. L. Hulbert, Many-Body Effects in Angle-Resolved Photoemission: Quasiparticle Energy and Lifetime of a Mo (110) Surface State, Phys. Rev. Lett. **83**, 2085 (1999).

[23] A. A. Kordyuk, S. V. Borisenko, A. Koitzsch, J. Fink, M. Knupfer, and H. Berger, Bare electron dispersion from experiment: Self-consistent self-energy analysis of photoemission data, Phys. Rev. B **71**, 214513 (2005).

[24] A. R. Adams, Band-structure engineering for low-threshold high-efficiency semiconductor lasers, Electron. Lett. **22**, 249 (1986).

[25] X. J. Zhou, T. Yoshida, A. Lanzara, P. V. Bogdanov, S. A. Kellar, K. M. Shen, W. L. Yang, F. Ronning, T. Sasagawa, and T. Kakeshita, High-temperature superconductors: universal nodal Fermi velocity, Nature (London) **423**, 398 (2003).

[26] I. M. Vishik, W. S. Lee, F. Schmitt, B. Moritz, T. Sasagawa, S. Uchida, K. Fujita, S. Ishida, C. Zhang, and T. P. Devereaux, Doping-Dependent Nodal Fermi Velocity of the High-Temperature Superconductor $Bi_2Sr_2CaCu_2O_{8+\delta}$ Revealed Using High-Resolution Angle-Resolved Photoemission Spectroscopy, Phys. Rev. Lett. **104**, 207002 (2010).

[27] E. Pavarini, I. Dasgupta, T. Saha-Dasgupta, O. Jepsen, and O. K. Andersen, Band-Structure Trend In Hole-Doped Cuprates and Correlation with T_c max, Phys. Rev. Lett. **87**, 047003 (2001).

[28] H. Lin, S. Sahrakorpi, R. S. Markiewicz, and A. Bansil, Raising Bi-O bands Above the Fermi Energy Level of Hole-Doped $Bi_2Sr_2CaCu_2O_{8+\delta}$ and Other Cuprate Superconductors, Phys. Rev. Lett. **96**, 097001 (2006).

[29] N. Pyka, W. Reichardt, L. Pintschovius, G. Engel, J. Rossat-Mignod, and J. Y. Henry, Superconductivity-Induced Phonon Softening in $YBa_2Cu_3O_7$ Observed by Inelastic Neutron Scattering, Phys. Rev. Lett. **70**, 1457 (1993).

[30] R. J. McQueeney, Y. Petrov, T. Egami, M. Yethiraj, G. Shirane, and Y. Endoh, Anomalous Dispersion of LO Phonons in $La_{1.85}Sr_{0.15}CuO_4$ at Low Temperatures, Phys. Rev. Lett. **82**, 628 (1999).

[31] H. F. Fong, P. Bourges, Y. Sidis, L. P. Regnault, A. Ivanov, G. D. Gu, N. Koshizuka, and B. Keimer, Neutron scattering from magnetic excitations in $Bi_2Sr_2CaCu_2O_{8+\delta}$, Nature (London) **398**, 588 (1999).

[32] Y. Zhong, Y. Chen, J. Guan, J. Zhao, Z. Rao, C. Tang, H. Liu, Y. Sun, and H. Ding, Extraction of tight binding parameters from in-situ ARPES on the continuously doped surface of cuprates, Sci. China: Phys., Mech. Astron. **61**, 127403 (2018).

[33] M. Hashimoto, T. Yoshida, H. Yagi, M. Takizawa, A. Fujimori, M. Kubota, K. Ono, K. Tanaka, D. H. Lu, and Z. X. Shen, Doping evolution of the electronic structure in the single-layer cuprate $Bi_2Sr_{2-x}La_xCuO_{6+\delta}$: Comparison with other single-layer cuprates, Phys. Rev. B **77**, 094516 (2008).

[34] A. B. Migdal, Interaction between electrons and lattice vibrations in a normal metal, Zh. Eksp. Teor. Fiz. **34**, 1438 (1958) [Sov. Phys. JETP **7**, 996 (1958)].

[35] K. M. Shen, F. Ronning, D. H. Lu, W. S. Lee, N. J. C. Ingle, W. Meevasana, F. Baumberger, A. Damascelli, N. P. Armitage, L. L. Miller *et al.*, Missing Quasiparticles and the Chemical Potential Puzzle in the Doping Evolution of the Cuprate Superconductors, Phys. Rev. Lett. **93**, 267002 (2004).

[36] A. S. Mishchenko, N. Nagaosa, K. M. Shen, Z. X. Shen, X. J. Zhou, and T. P. Devereaux, Polaronic metal in lightly doped high-Tc cuprates, Europhys. Lett. **95**, 57007 (2011).

[37] N. C. Plumb, T. J. Reber, J. D. Koralek, Z. Sun, J. F. Douglas, Y. Aiura, K. Oka, H. Eisaki, and D. S. Dessau, Low-Energy (<10 meV) Feature in the Nodal Electron Self-Energy and Strong Temperature Dependence of the Fermi

Velocity in $Bi_2Sr_2CaCu_2O_{8+\delta}$, Phys. Rev. Lett. **105**, 046402 (2010).

[38] T. Kondo, Y. Nakashima, W. Malaeb, Y. Ishida, Y. Hamaya, T. Takeuchi, and S. Shin, Anomalous Doping Variation of the Nodal Low-Energy Feature of Superconducting $(Bi, Pb)_2(Sr, La)_2CuO_{6+\delta}$ Crystals Revealed by Laser-Based Angle-Resolved Photoemission Spectroscopy, Phys. Rev. Lett. **110**, 217006 (2013).

[39] A. M. Merritt, J.-P. Castellan, T. Keller, S. R. Park, J. A. Fernandez-Baca, G. D. Gu, and D. Reznik, Low energy phonons in $Bi_2Sr_2CaCu_2O_{8+\delta}$ and their possible interaction with electrons measured by inelastic neutron scattering, Phys. Rev. B **100**, 144502 (2019).

[40] J. Voit, One-dimensional Fermi liquids, Rep. Prog. Phys. **58**, 977 (1995).

[41] B. J. Kim, H. Koh, E. Rotenberg, S. J. Oh, H. Eisaki, N. Motoyama, S. Uchida, T. Tohyama, S. Maekawa, and Z. X. Shen, Distinct spinon and holon dispersions in photoemission spectral functions from one-dimensional $SrCuO_2$, Nat. Phys. **2**, 397 (2006).

[42] P. W. Anderson and Z. Zou, "Normal" Tunneling and "Normal" Transport: Diagnostics for the Resonating-Valence-Bond State, Phys. Rev. Lett. **60**, 132 (1988).

[43] G. H. Gweon, J. W. Allen, and J. D. Denlinger, Generalized spectral signatures of electron fractionalization in quasi-one- and two-dimensional molybdenum bronzes and superconducting cuprates, Phys. Rev. B **68**, 195117 (2003).

[44] R. B. Laughlin, Evidence for Quasiparticle Decay in Photoemission from Underdoped Cuprates, Phys. Rev. Lett. **79**, 1726 (1997).

[45] D. Orgad, S. A. Kivelson, E. W. Carlson, V. J. Emery, X. J. Zhou, and Z. X. Shen, Evidence of Electron Fractionalization from Photoemission Spectra in the High Temperature Superconductors, Phys. Rev. Lett. **86**, 4362 (2001).

[46] P. A. Lee, N. Nagaosa, and X.-G. Wen, Doping a Mott insulator: Physics of high-temperature superconductivity, Rev. Mod. Phys. **78**, 17 (2006).

[47] M. Fujita, H. Hiraka, M. Matsuda, M. Matsuura, J. M. Tranquada, S. Wakimoto, G. Xu, and K. Yamada, Progress in neutron scattering studies of spin excitations in high-Tc cuprates, J. Phys. Soc. Jpn. **81**, 011007 (2011).

[48] P. W. Anderson, Spin-charge separation is the key to the high Tc cuprates, Physica C **341**, 9 (2000).

[49] S. A. Kivelson, D. S. Rokhsar, and J. P. Sethna, Topology of the resonating valence-bond state: Solitons and high-T_c superconductivity, Phys. Rev. B **35**, 8865 (1987).

[50] Z.-Y. Weng, Phase string theory for doped antiferromagnets, Int. J. Mod. Phys. B **21**, 773 (2007).

[51] D. N. Sheng, Y. C. Chen, and Z. Y. Weng, Phase String Effect in a Doped Antiferromagnet, Phys. Rev. Lett. **77**, 5102 (1996); Z. Y. Weng, D. N. Sheng, Y. C. Chen, and C. S. Ting, Phase string effect in the t-J model: General theory, Phys. Rev. B **55**, 3894 (1997).

[52] K. Wu, Z. Y. Weng, and J. Zaanen, Sign structure of the t−j model, Phys. Rev. B **77**, 155102 (2008).

[53] Z.-Y. Weng, Superconducting ground state of a doped Mott insulator, New J. Phys. **13**, 103039 (2011); Y. Ma, P. Ye, and Z.-Y. Weng, Low-temperature pseudogap phenomenon: precursor of high-Tc superconductivity, *ibid.* **16**, 083039 (2014).

[54] J.-H. Zhang, S. Li, Y. Ma, Y. Zhong, H. Ding, and Z.-Y. Weng, Phenomenological Description of the Spectral Function for the Pseudogap and Superconducting Phases of High-T_c Cuprates, arXiv:1905.04862.